Scientific paper

Exploring zingerone 2-thiohydantoins as anticancer agents against breast adenocarcinoma: Cytotoxicity, HSA and DNA binding, molecular docking and ADMET prediction

Petar B. Stanić,[1,*] Ana M. Rilak-Simović,[1] Katarina D. Virijević,[1] Jovana M. Muškinja,[1] Nevena S. Jeremić,[2,3,4] Goran V. Janjić,[5] Biljana M. Šmit[1]

[1] *Institute for Information Technologies, University of Kragujevac, Liceja Kneževine Srbije 1A, 34000 Kragujevac, Serbia*

[2] *Center of Excellence for Redox Balance Research in Cardiovascular and Metabolic Disorders, Svetozara Markovića 69, 34000 Kragujevac, Serbia*

[3] *Department of Pharmacy, Faculty of Medical Sciences, University of Kragujevac, Svetozara Markovića 69, 34000 Kragujevac, Serbia*

[4] *Federal State Autonomous Educational Institution of Higher Education, I. M. Sechenov First Moscow State Medical University of the Ministry of Health of the Russian Federation, 8-2 Trubetskaya str., 119991 Moscow, Russia*

[5] *Institute of Chemistry, Technology and Metallurgy, University of Belgrade, Njegoševa 12, 11000 Belgrade, Serbia*

* *Corresponding author: E-mail: petar.stanic@uni.kg.ac.rs*

Received: 11-22-25

Abstract

This study investigates a series of zingerone 2-thiohydantoins for anticancer activity towards human breast adenocarcinoma and explores possible mechanisms of anticancer action. Cytotoxicity was tested on highly invasive triple negative breast cancer MDA-MB-231 cells and healthy MRC-5 cells. The most active compound **2e** exerted a significant cytotoxic effect on breast cancer cells, while exhibiting no measurable toxicity on healthy cells. Fluorescence measurements of interactions with human serum albumin, combined with molecular docking, showed strong binding and transport capabilities, suggesting good bioavailability. Fluorescence and hydrodynamic measurements with DNA displayed lower binding affinity, suggesting that protein targets are responsible for anticancer action. Thorough molecular docking screening on 36 possible breast adenocarcinoma protein targets was performed and results suggest competitive inhibition of DNA methyltransferase 1 as the mechanism of anticancer action. ADMET analysis predicted favorable physicochemical and pharmacokinetic properties.

Keywords: hydantoin, ginger, cytotoxic, molecular docking, ADMET.

1. Introduction

Cancer as a whole represents a class of one of the most desolating and mortifying human diseases that leads to a death toll counting in the millions per year around the world.[1] It is a complex disease, encompassing a large list of diverse metabolic disorders and alterations of biomolecular mechanisms and signaling pathways. Breast cancer specifically has become the most common type worldwide, taking the first place from lung cancer as the most commonly diagnosed form of cancer. In 2022 alone there were 2.3 million new breast cancer cases globally among women, while 670000 of those cases had lethal outcomes.[2] Current medicine, although expanding in practice, is in dire need of new treatment options for this highly concerning and harmful disease.

There are several different strategies for treatment of breast cancer.[3] They vary through structure-activity relationship features and include modulation of certain receptors (like the human epidermal growth factor receptor 2 or estrogen and progesterone receptors), mutation of certain genes (for example breast cancer 1 gene or phosphatidylinositol-4,5-bisphosphate 3-kinase catalytic subunit alpha) and influence on certain biomarkers associated with tu-

mor microenvironment (for example tumor-infiltrating lymphocyte and programmed death ligand 1). This is important to consider from a rational drug design standpoint. Any new potential antitumor compound or class of compounds needs to have its molecular features thoroughly assessed in order to deduce its potential. Moreover, unraveling potential modes of its antitumor action leads to a better understanding of its activity and also, narrows down the search for new, more viable antitumor agents.

2-Thiohydantoins, sulfur analogues of a broader group of heterocyclic compounds called hydantoins, are a class of cyclic ureides, known for their various biological activities, low toxicity and uses in medicine and industry and have generally been a hot topic in drug discovery.[4–6] The hydantoin moiety is regarded as an important pharmacophore, as hydantoins express a wide variety of biological activities, such as anti-inflammatory,[7] antimicrobial,[8] anticonvulsant,[9] antidiabetic,[10] diabetes mellitus (DM antiplatelet,[11] anti-HIV[12] and, of course, anticancer.[13] Hydantoins have been reported to express anticancer activity in numerous different ways, whether through antiproliferative activity,[13] inhibition of certain enzymes, such as sirtuin, B-cell lymphoma-2,[14] androgen receptors,[15] NADPH oxidase,[16] isocitrate dehydrogenase,[17] DNA topoisomerase[18] or efflux pump P-glycoproteins[19] and are, as such, prospective potential anticancer agents.

Various hydantoins are used in therapeutic purposes and are commercially available, clinically approved drugs. Although hydantoins are mostly known in medicine for their use as anticonvulsants in the treatment of epilepsy,[20] a few have found use in cancer therapy. Nilutamide, apalutamide and enzalutamide are non-steroid antiandrogens that are used in the treatment of prostate cancer.[21–23] To date, these are the only hydantoins that have reached medical practice for cancer treatment of any sort. Considering the vast biological potential of these compounds and the ever-increasing demand for new anticancer drugs, there is a large gap that novel compounds from the hydantoin class can come into.

Combining different pharmacophores in one hybrid molecule is a powerful strategy in drug discovery, as it enables the targeting of various diseases. This hybrid approach is used to modulate biological activities and the resulting hybrid compounds most often experience an increase in the biological potential of at least one of the combined pharmacophores.[24] This framework is the perfect space in which the interplay of natural product chemistry and synthetic chemistry can occur, as deriving established biologically active natural products with synthetic pharmacophores can yield interesting results.[25] Zingerone, a naturally occurring methoxyphenol ginger extract, is known for its impressive pharmacological properties.[26] Both naturally occurring zingerone and its synthetic derivatives have been shown to possess various biological activities, such as anticancer, antimicrobial, antioxidant, anti-inflammatory, hepatoprotective etc. More importantly to the context of this study, zingerone has been shown to exert a potent cytotoxic effect on triple negative breast cancer cells.[27] Merging and linking zingerone and 2-thiohydantoin moieties could, by design, produce more bioactive structures with better pharmacological properties, which would include more potent activity, higher bioavailability and fewer toxic and other adverse side effects.

In our previous work, biological activities of a newly synthesized series of zingerone-thiohydantoin hybrid compounds were explored.[13] The compounds exhibited moderate antibacterial activities, but, more importantly, showed anticancer potential through antiproliferative activity against the colorectal cancer cell line HCT-116. The results prompted an expanded anticancer evaluation and the activity of the compounds was tested on the triple negative breast cancer cell line MDA-MB-231 and an investigation of the possible mechanisms of anticancer action was warranted, as well. Triple negative breast cancer is a particularly invasive form of cancer and it is reported to be the most difficult sort of breast cancer to treat and overcome.[28] The results of this study show a strong cytotoxic effect of the lead compound **2e** on the triple negative breast cancer cell line MDA-MB-231. Biomolecular mechanisms of anticancer action were investigated by analyzing interactions with DNA and human serum albumin, as well as molecular docking, to determine the most probable mode of its anticancer action. Physicochemical and ADMET parameters were analyzed in order to determine the pharmacokinetic and drug-likeness properties.

2. Experimental

2.1. Chemicals and reagents

Chemicals and reagents used in this study were commercially attained (Merck and Fisher Scientific) and were used as received, with no additional purification. Solvents were purified by distillation and dried with standard protocols prior to use. Zingerone, which is the starting substrate for the synthesis of *O*-alkyl zingerone derivatives **1a–g**, was not obtained commercially, but was instead synthesized from vanillin and acetone, according to a well-established condensation protocol.[29]

2.2. Instrumentation

IR spectra were recorded using potassium bromide pellets on a Perkin-Elmer FT-IR spectrometer, model Spectrum One, in the 4000 to 450 cm^{-1} working range. ^{1}H and ^{13}C NMR spectra were recorded using a Varian Gemini 2000 NMR spectrometer. The solvent used was deuterated chloroform ($CDCl_3$) and tetramethylsilane (TMS) was used as the internal standard. 1290 Infinity LC system (Agilent Technologies, Waldbronn, Germany) was used for the LC-HRMS analysis, connected to the Quadrupole Time-of-Flight mass detector (6550 iFunnel QTOF MS,

Agilent Technologies; Santa Clara, CA, USA), equipped with a dual spray Agilent Jet Stream (AJS) electrospray ion source. Elemental analysis was performed on an Elemental Vario ELIII CHNSO analyzer. Perkin Elmer LS 55 Fluorescence Luminescence Spectrometer was used for HSA and DNA binding measurements. Multiskan SkyHigh Microplate spectrophotometer was used for all cytotoxicity assays.

2.3. Synthetic procedures

The starting *O*-alkyl zingerone derivatives **1a-g** were synthesized by using established protocols available in literature.[30,31] The structure and purity of the compounds were verified using IR and NMR spectroscopy and all the spectral data is available in the Supplementary material to this paper.

The zingerone 2-thiohydantoin derivatives **2a–g** were synthesized by using a slightly modified previously published protocol.[32] The starting *O*-alkyl zingerone derivative **1a–g** (2 mmol) and thiosemicarbazide (0.182 g, 2 mmol) were mixed and heated in 30 mL of methanol under reflux for 3 h. The mixture was then left to cool off at ambient temperature. Ethyl chloroacetate (0.245 g, 2 mmol) and anhydrous sodium acetate (0.482 g, 6 mmol) were then added to the mixture *in situ* and the mixture was then heated under reflux for another 6 h. After the reaction was complete, the reaction mixture was first left to cool off at ambient temperature and then cold water was added, resulting in a precipitate of the zingerone 2-thiohydantoin product **2a–g**. The precipitate was filtered from the mixture, washed with hot water and then finally re-crystallized from hot methanol, resulting in a white, amorphous powder. The structure and purity of the obtained zingerone 2-thiohydantoin derivatives were verified using IR and NMR spectroscopy, as well as LC-HRMS and elemental analysis. Spectral and other data related to the characterization of the compounds is given in the Supplementary material to this paper.

2.4. Cytotoxic activity determination

Stock 5 mM solutions of the tested compounds were prepared by dissolving the synthesized derivatives in dimethyl sulfoxide (DMSO) and working concentration solutions (0.1, 1, 10, 50, 100 and 250 μM) were obtained by further dilution in the Dulbecco's Modified Eagle Medium (DMEM). The concentration of DMSO in the working solutions did not exceed 0.05%, which is reported to be non-toxic to cancer cells.[33]

Human breast adenocarcinoma (MDA-MB-231) and healthy human lung fibroblast (MRC-5) cell lines were procured from the European Collection of Authenticated Cell Cultures. The cells were cultured under humidified conditions in a complete medium, at 37 °C and 5% $CO0_2$. Detachment was achieved by using 0.25% trypsin–EDTA after the cells reached 70–80% confluence, after which seeding was done in 96-well flat-bottomed microtitre plates (1×10^4 cells/well). The cells were treated with 100 μL of compound solutions 24 h after cell seeding. The influence of the compounds on the viability of the cell lines was determined after 24 and 72 h using MTT (3-(4,5-dimethylthiazol-2-yl)-2,5-diphenyltetrazolium bromide) assay according to a standard protocol.[34] After incubation, 25 μL of 5 mg/mL MTT solution was added to every well, after which incubation was done at 37 °C for 2 h and then finally, 100 μL of DMSO was added. Cytotoxic activity was evaluated by performing absorbance measurements at the wavelength of 550 nm. Results are expressed as a percent of cell viability (%) and IC_{50} values (minimal inhibitory concentration that induces the death of half of the treated cells) were calculated by extrapolation from the dose curves obtained from the MTT results. For the positive control, 5-fluorouracil (5-FU) was used. All assays were done in triplicates. The magnitude of the correlation between tested variables was determined using statistical SPSS software (version 20, 2008, Chicago, IL, USA), along with the ANOVA test. A value of $p < 0.05$ was treated as a statistically significant difference between the control and the tested compounds. The IC_{50} values were calculated with the CalcuSyn software program.

2.5. DNA and HSA binding measurements

The interaction of the compound with calf thymus (CT) DNA was studied at 25 °C by UV-Vis spectroscopy. The spectrophotometric titration was performed in PBS buffer (10 mM, c_{NaCl} = 137 mM, c_{KCl} = 2.7 mM, pH = 7.4) using a fixed complex concentration (13.0 μM), to which increasing amounts of the DNA stock solution were added (2.5 mM) and acquiring spectra in the 200–700 nm region with a 2 min equilibrium time. Concentrated stock solution of compound was prepared in dimethyl sulfoxide and then diluted to the required concentrations. The stock solution of CT DNA was prepared in 10 mM PBS and left for appropriate hydration overnight, which gave a ratio of UV absorbances at 260 nm and 280 nm (A260/A280) of *ca*. 1.8–1.9, indicating that the DNA was sufficiently free of protein. The concentration was determined by UV absorbance (ε = 6600 M^{-1} cm^{-1}) at 260 nm.[35] A fluorescence binding assay was performed by measuring the fluorescence quenching of ethidium bromide (EB) intercalated to CT DNA (5.5×10^{-5} M CT DNA and EB) in the absence and presence of increasing concentrations of compound (0–5.5×10^{-5} M). Emission spectra were recorded in the 550–750 nm region with excitation wavelength at 527 nm in 10 mM PBS buffer pH 7.4. The excitation and emission slit widths (each 10 nm) and scan rate were maintained constant throughout. Furthermore, the viscosity of a DNA solution was measured in the presence of increasing concentrations of the studied compound. The results were presented as $(\eta/\eta_0)^{1/3}$ against r, where η is the viscosity of

the DNA solution in the presence of the compound, and η_0 is the viscosity of the DNA solution in buffer alone.

The protein binding study was performed through tryptophan fluorescence quenching experiments using human serum albumin (HSA, 2.0 μM) in 10 mM PBS buffer (pH = 7.4). Titration experiments were carried out at 25 °C by adding the microliter amounts (4.0–40.0 μL) of a stock solution of the compound to the protein solution (2.0 mL) with an equilibration time of 2 min. The fluorescence spectra were recorded in the 300–500 nm range with excitation wavelength at 295 nm. Under the same experimental circumstances, the fluorescence spectra of the compound in buffered solution were recorded, but no fluorescence emission was detected. Furthermore, we have conducted competitive HSA-interactions with the site markers eosin Y, which serves as a marker for site I of the subdomain IIA, and ibuprofen, which serves as a marker for site II of the subdomain IIIA.[36] The fluorescence emission range was between 300 and 500 nm, with the excitation wavelength set at 295 nm. Equimolar amounts of HSA and markers (2.0 μM) were added to the solutions. The investigated compound was added in increasing concentrations up to 20.0 μM.

2.6. Computational methods

The structures of the investigated compounds were optimized by using Gaussian09 software,[37] with the B3LYP method and the 6-311++g** basis set.

AutoDock Vina was used for molecular docking calculations.[38] Docking was performed on whole biomolecules, and not on separate parts of the biomolecules, such as the active sites. The docking study includes whole biomolecules because there is no experimental data that determines the binding sites of the tested compounds. Crystal structures of the examined biomolecules were obtained from the Protein Data Bank.[39] The structures extracted from the Protein Data Bank were prepared for the docking study by removing co-crystalized water molecules and other ligands. BIOVIA Discovery Studio was used for visualization of target-ligand interactions.[40]

Physicochemical, drug-likeness and ADMET properties were assessed by using the SwissADME tool (http://www.swissadme.ch/)[41] and the resources from the pkCSM online server (https://biosig.lab.uq.edu.au/pkcsm/prediction).[42]

3. Results and discussion

3.1. Synthesis of the zingerone 2-thiohydantoin derivatives

Zingerone 2-thiohydantoin derivatives **2a–g** were synthesized through a two-step coupling reaction (Scheme 1).[13] First the starting *O*-alkyl zingerone derivatives **1a–g** underwent a condensation reaction with thiosemicarbazone, giving intermediate thiosemicarbazones. The thiosemicarbazones then underwent cyclization with ethyl chloroacetate in the presence of anhydrous sodium acetate, finally yielding the zingerone 2-thiohydantoin derivatives **2a–g**. All compounds were synthesized in medium to high yields (61–88%), except **2d**, which was synthesized in a modest 33% yield. The structures and purities of the compounds were verified with NMR and IR spectroscopy, as well as LC-HRMS and elemental analysis (spectra and spectral data are given in the Supplementary material).

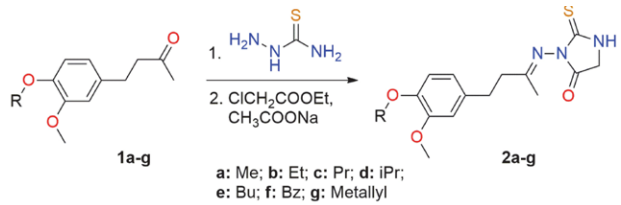

Scheme 1. Synthesis of zingerone 2-thiohydantoin derivatives.

3.2. Cytotoxic activity of the zingerone 2-thiohydantoin derivatives towards human breast adenocarcinoma

In order to examine anticancer potential of the zingerone 2-thiohydantoin derivatives **2a–g** for breast adenocarcinoma, cytotoxic activity of the compounds was tested on the triple negative breast cancer MDA-MB-231 cell line. Cytotoxicity of the compounds was tested on MRC-5 cells, as well, in order to determine their effect on the viability of healthy cells. 5-Fluorouracil (5-FU), a commercially available cytotoxic chemotherapeutic, was used as the positive control. 5-FU interferes with DNA replication and is used through intravenous injection for the treatment of various different types of cancer, including pancreatic, stomach, colorectal, cervical, and, of course, breast cancer.

Cytotoxic effects of the zingerone 2-thiohydantoin derivatives **2a–g** were expressed through viability *vs.* dose curves (Figures S43 and S44) and IC_{50} values (Table 1). A notable decrease in MDA-MB-231 cell viability was observed mostly after 72 h, while a notable decrease in viability after 24 h was observed only for **2e**, where cell viability fell slightly under 60% in the concentration range above 100 μM. After 72 h, 2-thiohydantoin derivative **2e** substantially reduced cell viability in the tested concentration range and exerted a significant cytotoxic effect with an $IC_{50}{}^{72\,h}$ of 31.86 μM. Unlike other derivatives and 5-FU, only **2e** exhibited a light, but noticeable 20% reduction effect on MDA-MB-231 cell viability at the lowest tested concentration of 0.1 μM. The dose-response curve does, however, plateau up until 10 μM, after which a sharper decrease in cell viability is observed. Besides **2e**, derivative **2c** exhibited a moderate effect with an $IC_{50}{}^{72\,h}$ value of 164.41

μM. Both of them exerted a greater cytotoxic effect than the control, 5-fluorouracil. Out of all the examined compounds in the series, only **2a** exhibited any cytotoxicity towards healthy MRC-5 cells in the tested range, with an $IC_{50}^{72\ h}$ value of 184.15 μM after 72 h and the control, 5-fluorouracil with an $IC_{50}^{72\ h}$ value of 181.71 μM. In the case of **2e**, only a slight reduction in cell viability of about 20% is observed after 24 h at the highest tested concentrations, while after 72 h, there is no significant reduction of healthy MRC-5 cell viability in the tested concentration range.

The results demonstrate the leading compound **2e** exhibits a significant cytotoxic effect on the triple negative breast cancer MDA-MB-231 cell line, while having no effect on the viability of healthy MRC-5 cells in the tested concentration range, up to 250 μM, showing good selectivity. As the leading compound shows promising activity, further evaluation of its interactions with important biomolecules was performed in order to uncover possible mechanisms of action and assess its anticancer potential.

Table 1. Cytotoxic effects of the zingerone 2-thiohydantoin derivatives **2a–g** and 5-fluorouracil on the triple negative breast cancer MDA-MB-231 cells and healthy MRC-5 cells after 72 h of exposure, expressed in IC_{50} values, with calculated selectivity index (SI) values.

Compound	IC_{50} / μM		
	MDA-MB-231	MRC-5	SI
2a	>250	184.15 ± 0.54	<0.74
2b	>250	>250	n.d.
2c	164.43 ± 0.29	>250	>1.52
2d	>250	>250	n.d.
2e	**31.86** ± 0.18	>250	**>7.85**
2f	>250	>250	n.d.
2g	>250	>250	n.d.
5-FU	>250	181.71 ± 0.69	<0.73

3.3. Interactions with human serum albumin

The interactions between potential drugs and serum albumin, the most abundant protein in plasma, may increase or limit their pharmacological effects or provide paths for drug transportation.[43] Many drugs are synthesized to target specific proteins, and targeting often means inhibition of protein activity. HSA is the most abundant protein in plasma and a dominant transport biomacromolecule, and accommodates a wide range of lipophilic ligands because of its highly flexible three-dimensional structure.[44] The interactions of **2e** with HSA were examined by fluorescence spectroscopy as this method allows a quantitative assessment of the binding strength. HSA possesses a single tryptophan residue, Trp214, and λ_{exc} = 295 nm is used in order to excite the Trp residue. Trp214 is located near Sudlow site I, but it seems that Trp214 can even indicate changes occurring in the druggable site II in subdomain IIIA.[43] Addition of **2e** to the HSA solution (up to r values of 10) results in a significant quenching of HSA fluorescence at λ = 335 nm in a concentration-dependent manner (Figure 1a). Ten molar excess of **2e** quenched the fluorescence to approximately 25% of the initial value. Meanwhile, a significant blue shift of the maximum emission wavelength from 335 to 330 nm was also observed, suggested that the polarity of the protein environment was changed in the presence of **2e**.[45] The measured fluorescence intensities were subjected to Stern–Volmer equation (1):[46]

$$I_0/I = 1 + k_q \tau_0 [Q] = 1 + K_{SV}[Q] \quad (1)$$

where I_0 and I are the tryptophan fluorescence intensities of HSA in the absence and presence of the quencher (**2e**), respectively; K_{SV} is the Stern–Volmer quenching constant; k_q is the bimolecular quenching constants; τ_0 is the average lifetime of fluorophore without the quencher; [Q] is the concentration of quencher. The Stern–Volmer plot was linear (Figure 1b) up to at least 10-fold excess of **2e** over HSA, suggesting a predominant involvement of one type of quenching in the interaction. K_{SV} (1.36×10^5 M^{-1}) was obtained from the slope of the linear plot, while k_q (1.36×10^{13} M^{-1} s^{-1}) was calculated from K_{SV} using equation (1) and assuming τ_0 = 6 ns for HSA.[47] The values of these constants indicate a significant quenching ability of the HSA fluorescence. Moreover, the value of k_q was three orders of magnitude greater than the maximum diffusion constant of biomolecules (2×10^{10} M^{-1} s^{-1}), thereby suggesting the predominance of static quenching, i.e., the formation of drug–HSA adducts.[46]

The values of the HSA-binding constant (K) and the number of binding sites per albumin (n), were calculated from the Scatchard equation (2):[48]

$$r/D_f = nK - rK \quad (2)$$

where r ($r = \Delta I/I_0$) is the mole of **2e** bound per mole of protein, and D_f is the molar concentration of free **2e**. The association binding constant K was calculated from the slope in the Scatchard plot r/D_f *vs.* r (Figure 1c), and the number of binding sites per albumin (n) was given by the ratio of the y intercept to the slope. The K value (2.8×10^5 M^{-1}) indicates a strong binding affinity of **2e** to HSA and the n value (n = 0.87) suggests that there is only one binding site available on the protein. Furthermore, this finding suggests that **2e** would be bound to HSA strongly enough to allow transfer and release from HSA upon arrival at the target cells.

3.3.1. Fluorescence titration

Since the spectrofluorimetric quenching studies cannot give information on whether the binding mode of drugs to HSA is noncovalent or coordinative, a fluores-

cence titration method involving particular site markers, eosin Y as a marker for site I of subdomain IIA, and ibuprofen as a marker for site II of subdomain IIIA, was applied to probe the nature of the preferred binding site and to specify the affinity of **2e** for the protein.[49] The excitation wavelength for the fluorescence titration was 295 nm, with the emission range of 300–500 nm (Figures 1d-f and 1g-i). HSA and the markers were added in equimolar concentrations (2 μM). Then, the solution of **2e** was gradually added with increasing concentrations, up to a ratio of 10.

The Stern–Volmer (K_{SV}), bimolecular quenching (k_q) and binding constants (K) for the interactions with HSA in the absence and presence of site markers are depicted in Table 2. There is no discernible difference in the binding affinities of **2e** with either site markers, or with HSA alone. The compound exhibited high binding affinity in all three cases. Moreover, upon analyzing the plot relative fluorescence intensity, shown in Figure 1j, fluorescence intensities drop with an increased concentration ratio in a nearly identical manner in all three cases, indicating a matching quenching mechanism. The results suggest a third binding site in all three cases, which likely corresponds to drug site III, located in subdomain IB, which is recognized in literature as a major drug binding site.[50]

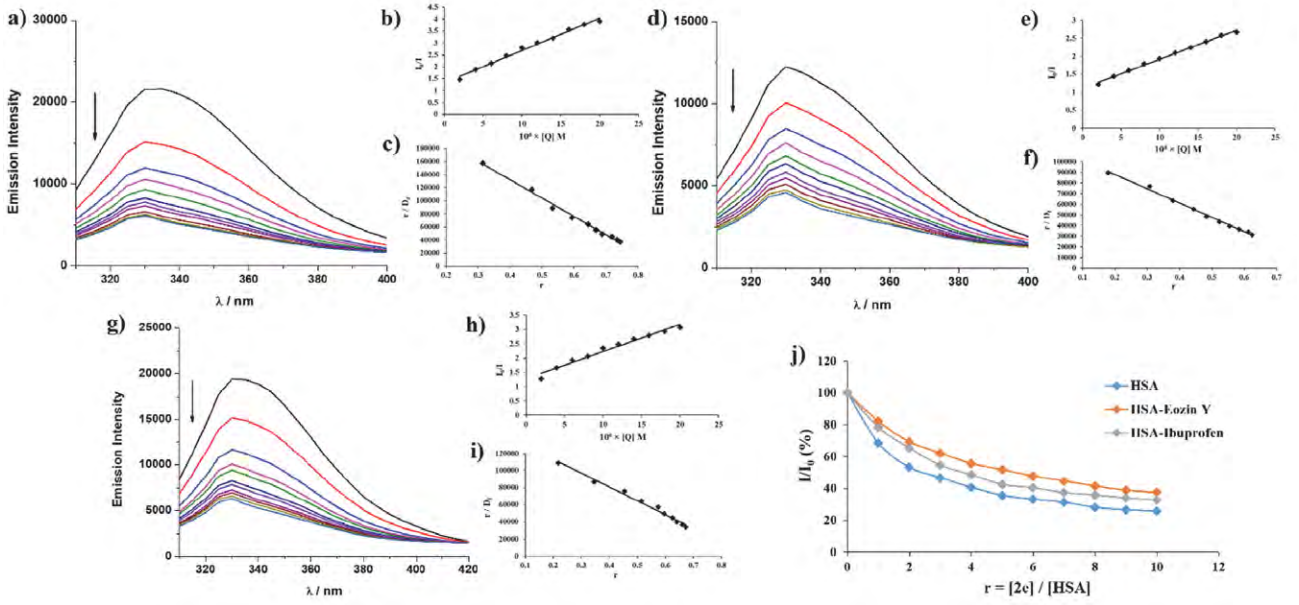

Figure 1. a) Emission spectra of HSA in the presence of **2e**. [HSA] = 2 μM, [**2e**] = 0–20 μM; λ_{ex} = 295 nm. Arrow shows the changes in intensity upon increasing the concentration of **2e**; b) Stern-Volmer plot of HSA for **2e**; c) Scatchard plot of HSA for **2e**; d) Emission spectra of HSA-eosin Y in the presence of **2e**. [HSA] = 2 μM, [eosin Y] = 2 μM, [**2e**] = 0–20 μM; λ_{ex} = 295 nm; e) Stern-Volmer plot of HSA-EosinY for **2e**; f) Scatchard plot of HSA-Eosin Y for **2e**; g) Emission spectra of HSA-ibuprofen in the presence of **2e**. [HSA] = 2 μM, [ibuprofen] = 2 μM, [**2e**] = 0–20 μM; λ_{ex} = 295 nm; h) Stern-Volmer plot of HSA-ibuprofen for **2e**; i) Scatchard plot of HSA-Ibuprofen for **2e**; j) Plot of relative fluorescence intensity at λ_{em} = 335 nm (%) *vs.* r (r = [**2e**]/[HSA]) for **2e** (25 % of the initial fluorescence intensity for HSA, 37 % for HSA-eosin Y and 32% for HSA-ibuprofen, respectively) in PBS buffer.

The HSA–site marker adducts, HSA–eosin Y and HSA–ibuprofen, show intense emission and their displacement by **2e** from the binding pocket of the protein is accompanied by a considerable decrease in the emission intensity. Ten molar excess of **2e** quenched the fluorescence to approximately 37% and 3% of the initial value for HSA–eosin Y and HSA–ibuprofen, respectively (Figure 1j). The emission quenching data were analyzed according to the Stern–Volmer equation (1) and Scatchard equation (2).[46,48]

3.3.2. Molecular docking

A molecular docking study was performed in order to help determine binding modes of the lead compound **2e**

Table 2. HSA constants (K_{SV}, k_q, K, n) for the interactions of **2e** in the absence and presence of eosin Y or ibuprofen.

System	K_{SV} [M^{-1}]	k_q [$M^{-1} s^{-1}$]	K [M^{-1}]	n
No site marker	$(1.4 \pm 0.1) \times 10^5$	$(1.4 \pm 0.1) \times 10^{13}$	2.8×10^5	0.87
HSA-eosin Y	$(8.0 \pm 0.2) \times 10^4$	$(8.0 \pm 0.20) \times 10^{12}$	1.4×10^5	0.85
HSA-ibuprofen	$(9.5 \pm 0.1) \times 10^4$	$(9.5 \pm 0.1) \times 10^{12}$	1.8×10^5	0.88

to human serum albumin. A structure of the protein deposited to the Protein Data Bank with the PDB ID 4L8U was used for the calculations.[51] Two probable binding sites were identified (Figure 2, left). The first binding site (BS1, –9.4 kcal mol^{-1}) is located in subdomain IB, known as the drug site III. The second binding site (BS2, –9.2 kcal mol^{-1}) is located in the space between subdomains IIA and IIIA. The results show that **2e** has a slightly higher binding affinity towards BS1 over BS2.

In BS1, **2e** interacts with amino acids from the α-helices and random coil in subdomain IB (Figure 2, right). The compound has only one donor group and five acceptor groups for classical hydrogen bonding. Nevertheless, only the N-H and thiocarbonyl groups from the 2-thiohydantoin form hydrogen bonds, the rest are unsatisfied. There are also two non-classical, carbon-hydrogen and Pi-donor hydrogen bonds. Other interactions include hydrophobic π/sulfur, π/alkyl, π/π and alkyl/alkyl interactions.

In BS2, only the oxygen from the methoxy group forms a hydrogen bond (Figure S45). The 2-thiohydantoin moiety does not seem to form any sort of interactions with the protein. The bulk of the interactions include π/alkyl interactions of the benzene ring and hydrophobic interactions of the carbon side chains.

The results of the molecular docking investigation are in accordance with the results obtained experimentally by fluorescence spectroscopy, as they suggest that the drug site III in subdomain IB is the main binding site of **2e**. The second binding site, BS2, although only slightly less favorable than BS1, is not a drug transporting site. The binding of **2e** in BS1 would ensure its bioavailability and a sufficiently strong interaction to be transported and released upon targeted cancer cells.

3.4. Interactions of the zingerone 2-thiohydantoin derivatives with DNA

The cellular target for many potential drugs is double-stranded helical DNA that can undergo a variety of changes.[52] Covalent DNA binding as an irreversible process causes permanent changes in the secondary structure of DNA and inhibits DNA processes and cell death. Noncovalent bonding involves electrostatic, intercalative, and groove-binding interactions.[53] UV–Vis spectroscopy is widely used to gain an initial understanding of a drug–DNA interaction by inspecting variations in the absorption of the drug species after successive DNA additions. The binding affinity of **2e** was evaluated by following the changes in its absorption spectrum upon increasing the concentration of CT DNA (Figure 3a). The addition of increasing amounts of CT DNA caused hyperchromism in the main absorption band of **2e** at 273 nm. Hyperchromism suggested a moderate binding affinityof **2e** to CT DNA. In order to quantitatively determine the binding strength of **2e**, the intrinsic binding constants K_b were calculated using the following equation (3):[54]

$$[DNA]/(\varepsilon_A - \varepsilon_f) = [DNA]/(\varepsilon_b - \varepsilon_f) + 1/[K_b(\varepsilon_b - \varepsilon_f)] \quad (3)$$

where K_b is given by the ratio of slope to the *y* intercept in plots $[DNA]/(\varepsilon_A - \varepsilon_f)$ *vs* [DNA] (Figure 3b), [DNA] is the concentration of DNA in base pairs, $\varepsilon_A = A_{obsd}/[\mathbf{2e}]$, ε_f is the extinction coefficient for the unbound **2e** and ε_b is the

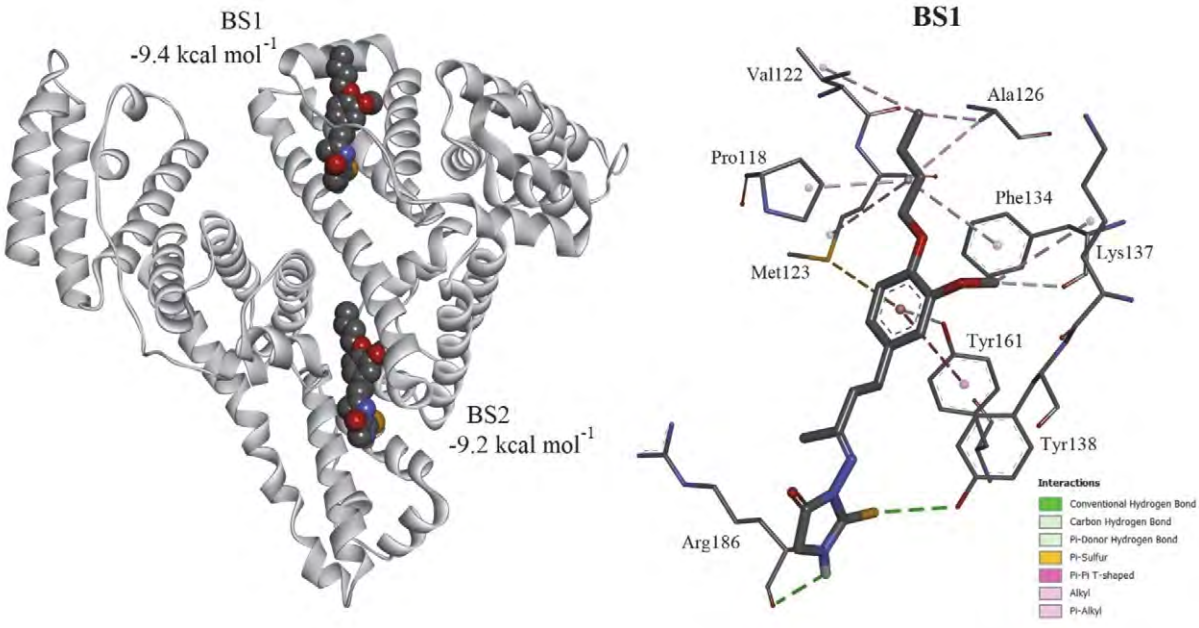

Figure 2. Left: Binding sites of **2e** in HSA. BS1 is the drug transport site III and BS2 is the non-transporting site between subdomains IIA and IIIA; Right: Amino acid environment and interactions of **2e** in drug site III (BS1) of HSA.

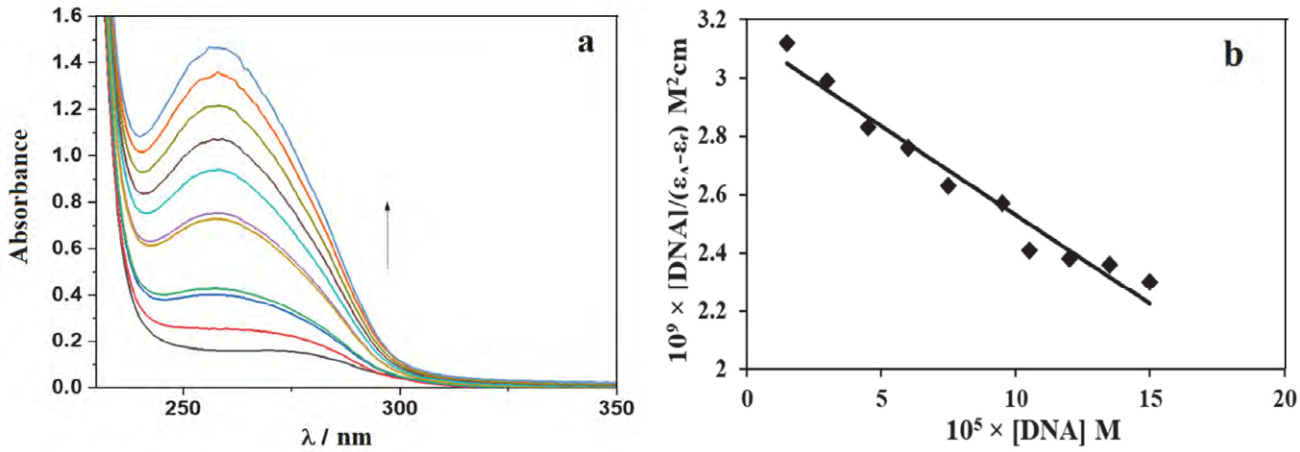

Figure 3. a) Absorption spectra of **2e** in PBS buffer upon addition of CT DNA. [*Q*] = 1.25 × 10^{-5} M, [DNA] = (0.12–1.25) × 10^{-5} M. Arrow shows the absorbance changing upon increasing DNA concentrations; b) Plots of [DNA]/($\varepsilon_A - \varepsilon_f$) *vs.* [DNA] for **2e**.

extinction coefficient for **2e** in the fully bound form. The intrinsic binding constants K_b of **2e** was (2.1 ± 0.1) × 10^3 M^{-1} suggesting a moderate binding affinity to CT DNA.

It is generally known that ethidium bromide (EB = 3,8-diamino-5-ethyl-6-phenylphenanthridinium bromide) acts as a CT DNA intercalator through the planar EB phenanthridine ring. Due to this intercalation and formation of the EB–CT DNA adduct, intense fluorescence emission occurs at 612 nm, when excited at 527 nm. Since the addition of compounds, which are able to intercalate DNA with the same or greater affinity than EB, may result in a decrease in fluorescence emission of the EB–CT DNA adduct, changes in the spectra obtained with EB when bound to DNA are frequently used for the study of intercalative binding of potential drugs to DNA. When excited at 527 nm, **2e** does not show any significant fluorescence at room temperature in solution or in the presence of CT DNA or EB. The addition of increasing amounts (up to r = 1.0) of the compound resulted in a slight decrease in the emission intensity band at 612 nm, indicating a weak competition of **2e** with EB in binding to DNA (Figure 4a). Being displaced from CT DNA, EB fluorescent emission dropped to 87% of its initial value (I_0) (Figure 4c).

Considering this observation, it can be concluded that the binding of **2e** to CT DNA resulted in a slight ejection of EB from the EB–CT DNA adduct. Additionally, quenching mechanism can be predicted from Stern–Volmer plots I_0/I vs. [*Q*] (Figure 4b) using Stern-Volmer equation (4):[46]

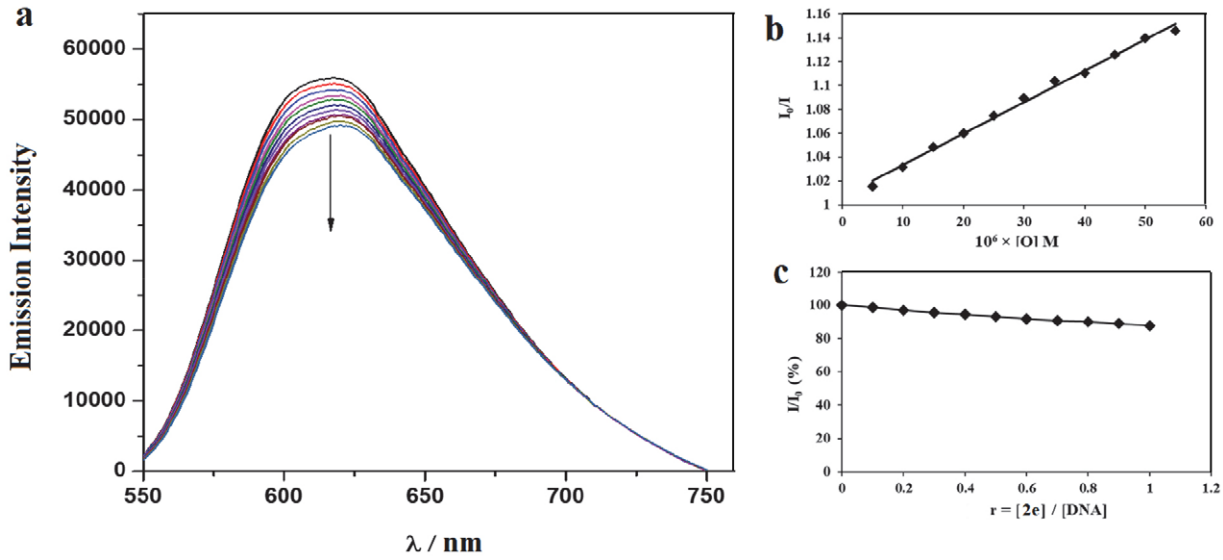

Figure 4. a) Emission spectra of EB bound to DNA in the presence of **2e**. [EB] = 55 μM, [DNA] = 55 μM; [Ru] = 0–55 μM; λ_{ex} = 527 nm. An arrow shows the intensity changes upon increased concentrations of **2e**; b) Stern-Volmer quenching plot of EB–DNA for **2e**; c) The relative intensity of fluorescent emission of EB at λ_{em} = 612 nm (λ_{ex} = 527 nm) *vs.* r (r = [**2e**]/[CT DNA]) for **2e** in 10 mM PBS (137 mM NaCl, pH 7.4).

$$I_0/I = 1 + K_{SV}[Q] \quad (4)$$

where I_0 and I are the emission intensities in the absence and the presence of the quencher, [Q] is the total concentration of quencher, K_{SV} is the dynamic quenching constant. The Stern–Volmer constant, K_{SV}, is calculated from the slope of the linear plot and is $(2.7 \pm 0.2) \times 10^3$ M^{-1}. The observed weak quenching of EB–DNA fluorescence suggests an interaction with CT DNA through minor groove binding rather than an intercalative mode.[55,56]

3.4.1. Viscosity measurements

When optical approaches fail to furnish adequate data to substantiate the binding mode, hydrodynamic tests, like viscosity measurements, serve as a crucial assessment for investigating the interactions with DNA. The classical intercalation of moieties into DNA results in a substantial rise in the viscosity of a DNA solution. Compounds that engage with DNA by electrostatic or groove interactions exhibit significantly diminished or negligible effects on the viscosity of DNA solutions.

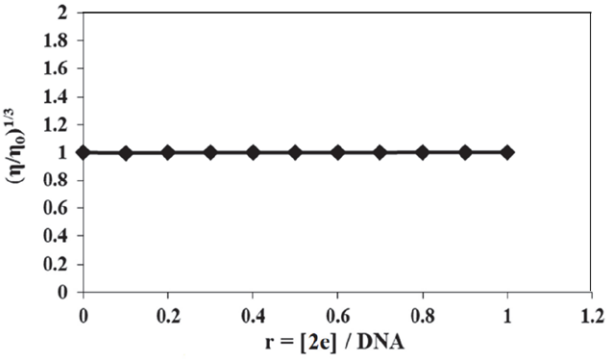

Figure 5. Relative viscosity $(\eta/\eta_0)^{1/3}$ of CT DNA (0.01 mM) in 10 mM PBS in the presence of the increasing amounts of **2e** (*r*).

Successive additions of **2e** had no measurable effect on the viscosity of the DNA solution (Figure 5). This in combinations with other DNA binding measurements suggests that the only likely DNA binding mode of **2e** would be groove binding. Overall, the results show that **2e** has a better binding affinity to HSA than to DNA, suggesting that protein targets seem to play a more important role than DNA in its anticancer activity.

3.5. Screening for probable breast adenocarcinoma biomolecular targets

As the results indicate that protein targets are more likely to be responsible for the anticancer activity of **2e**, a molecular docking screening was performed on 36 possible protein targets. These targets are specific proteins within signaling pathways that play a role in breast cancer growth, survival and spread and include Bcl-2, phosphoinositide 3-kinase, cyclin-dependent kinases, tumor necrosis factors and more. These protein targets were identified from available published literature and explanations as to how each of them are responsible for the survival and progression of triple negative breast cancer are given in the Supplementary Material. Along with the leading compound **2e**, an inactive compound **2a** was also docked in order to compare binding modes and determine the most likely target, based on the difference in the binding affinities.

The molecular docking results for most of the targets have been inconclusive, as there was no discernible difference in the binding modes of the active and inactive compound (Supplementary material, Tables S2 and S3). However, in the case of DNA methyltransferase 1 (DNMT1), a key difference was observed. DNMT1 catalyzes a site-specific methylation of DNA.[57] A methyl group is transferred from the substrate *S*-adenosyl-L-methionine to cytosine in the CpG site of the genome. The cytosine methylation changes gene expression and a regular methylation process maintains genome stability. However, unregulated methylation patterns lead to abnormal cell development and contribute to the proliferation and survival of cancer cells. Unregulated DNMT1 activity also silences tumor suppressor genes. For these reasons, DNMT1 is an important target in breast cancer therapy.[58]

The structure of DNA methyltransferase 1 deposited to the Protein Data Bank with the PDB ID 4DA4 was used for the calculations.[59] Two binding sites were identified for the active compound **2e** (Table 3 and Figure 6, left). The first binding site (BS1, –8.2 kcal mol^{-1}) is a non-inhibitory site, while the second binding site (BS2, –7.6 kcal mol^{-1}) is located in the active methyltransferase domain, meaning that **2e** could inhibit DNMT1 competitively. The native ligand, *S*-adenosyl-L-homocysteine (SAH), was redocked into catalytic site and it has a binding affinity of –8.1 kcal mol^{-1}, comparable to that of **2e**, only slightly higher. This is probably because DNMT1 in the obtained structure, already crystallized with SAH is conformationally adjusted to binding with SAH. The inactive **2a** only binds to the non-inhibitory site BS1, indicating a distinctive difference in their binding affinities and inhibitory activities. The results suggest that the binding of **2e** in the active center of DNMT1 could be responsible for its anticancer activity, while the inactivity of **2a** could be explained by its stronger affinity to the non-inhibitory site BS1.

Analysis of the amino acid environment reveals that the binding of **2e** in the active site (Figure 6, right) does indeed lead to interactions with key amino acid residues responsible for the methyl transfer process, such as the nucleophilic cysteine (Cys1229) that binds covalently to cytosine. The carbonyl oxygen from the 2-thiohydantoin ring forms two conventional hydrogen bonds with the catalytic cysteine, as well as a carbon hydrogen bond with the adjacent proline (Pro1228). The NH group from the 2-thiohydantoin ring also forms a classical hydrogen bond,

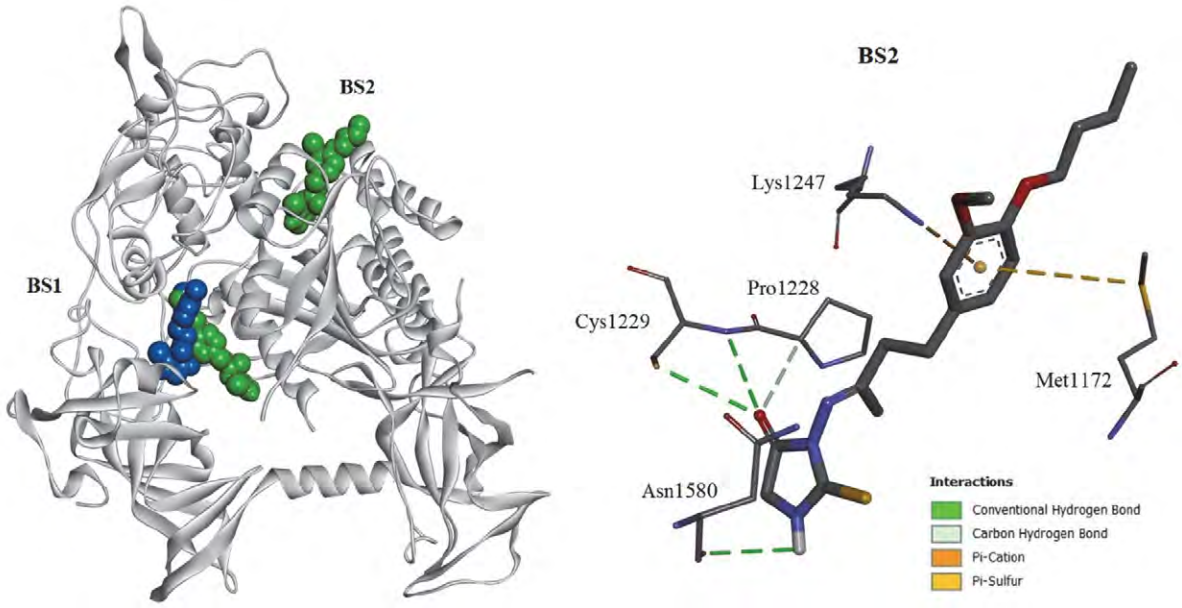

Figure 6. Left: Binding sites of **2e** (green) and **2a** (blue) in DNMT1. BS1 is a non-inhibitory site and BS2 is the catalytic methyl transfer site; Right: Amino acid environment and interactions of **2e** in the active site BS2 of DNMT1.

while the benzene ring is involved in π/sulfur and cationic/π interactions. Interactions of **2e** with catalytic elements of the active site further illustrate its DNMT1 inhibiting activity.

Table 3. Binding free energies (ΔG / kcal mol^{-1}) and binding sites of investigated compounds for DNA methyltransferase 1.

Ligand	Non-inhibitory site (BS1)	Active site (BS2)
2e	–8.2	–7.6
2a	–8.6	
S-adenosyl-L-homocysteine		–8.1

3.6. Drug-likeness and ADMET properties

To assess pharmacokinetic parameters and drug-likeness of the lead candidate, compound **2e**, ADMET analysis was performed. Physicochemical properties of compound **2e** are presented in Table 4 and the parameters are in accordance to Lipinski, Ghose, Veber, Egan and Muegge filters, indicating acceptable predicted levels of oral bioavailability. The six physicochemical parameters relevant to the bioavailability test (size, polarity, solubility, unsaturation, flexibility and lipophilicity) are in the acceptable range and are located in the desirable pink zone of the bioavailability radar (Figure 7), indicating adequate levels of predicted oral bioavailability.

Predicted pharmacokinetic properties of compound **2e** are presented in Table 5. The analysis revealed good permeability across the Caco-2 barrier and high intestinal

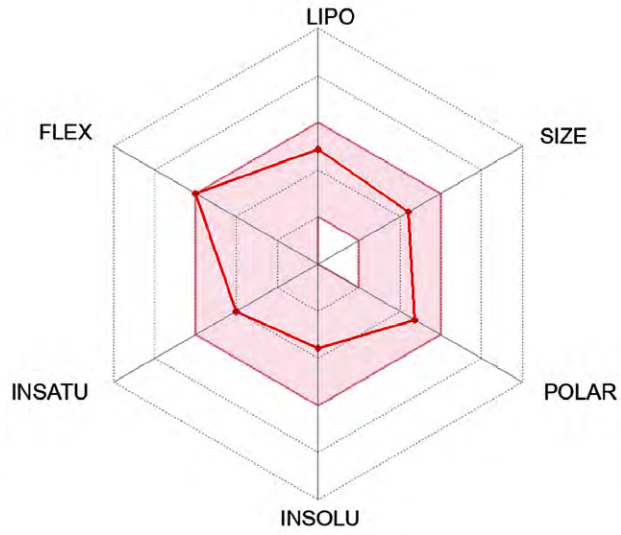

Figure 7. Bioavailability radar for compound **2e**.

Table 4. Physicochemical properties and drug-likeness of compound **2e**.

Molecular weight	363.47 g/mol
Number of heavy atoms	25
Number of aromatic heavy atoms	6
Fraction Csp3	0.50
Number of rotatable bonds	9
Number of H-bond acceptors	6
Number of H-bond donors	1
Molar refractivity	110.74
Total polar surface area	95.25 Å^2
Log *P*	2.95

absorption. The compound has low predicted blood-brain barrier and central nervous system permeability capabilities. This is better illustrated by Egan's boiled egg model (Figure 8), where it shown that the compound occupies the white part of Egan's egg and is very likely to be absorbed by the gastrointestinal tract passively and highly unlikely to cross the blood-brain barrier.

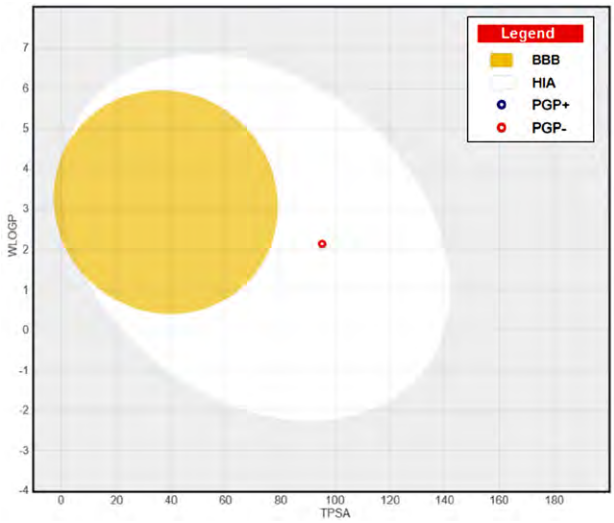

Figure 8. Egan's predictive boiled egg model for compound **2e**.

Metabolism assessment of the compound predicts that the compound is a substrate of cytochrome 3A4 and inhibitor of cytochrome 2C9, while having no effect on other key CYP enzymes. This, however, indicates a possibility of some drug-drug interactions. Elimination assessment predicts low total clearance and unlikeliness to be a substrate of the renal OCT2 transporter. Toxicity assessment predicts no AMES genotoxic effects. The compound is not an inhibitor of hERG I and II and poses no cardiovascular risk. A possibility of some hepatotoxic effects is predicted, while the analysis shows no possibility of skin sensitisation. The overall data indicates favorable physicochemical and "drug-like" characteristics and suitable pharmacokinetic properties of **2e**.

4. Conclusions

This study presents a combined effort in the evaluation of zingerone 2-thiohydantoin derivatives as anticancer agents against human breast adenocarcinoma. Highly invasive triple negative breast adenocarcinoma cells, MDA-MB-231 were chosen and the most active compound **2e** exhibited a significant cytotoxic effect with an IC_{50} of 31.86 μM, while having no measurable effect on healthy MRC-5 cells, showing good selectivity. Fluorescence spectroscopy measurements, combined with molecular docking, showed strong binding affinity of **2e** to human serum albumin, suggesting good transportcapabilities and bioavailability. The results suggest that the drug site III in HSA is the main binding and transport site. The binding affinity of **2e** to DNA was shown to be comparatively weaker, suggesting that protein targets are more likely to be responsible for its anticancer action. A molecular docking screening of 36 possible protein targets for breast adenocarcinoma suggests competitive inhibition of DNA methyltransferase 1 as the mechanism of anticancer action of **2e**. ADMET evaluation predicts favorable pharmacokinetic and "drug-like" properties of **2e**, most notably good bioavailability and low toxicity.

Targeted therapy for triple negative breast adenocarcinoma is exceedingly difficult and has not been developed

Table 5. Prediction of ADMET properties of compound **2e**.

Property	Model name	Predicted value
Absorption	Caco-2 permeability	0.909 log Papp in 10^{-6} cm/s
	Intestinal absorption	93.098%
Distribution	Blood-brain barrier permeability	–0.109 log BB
	Central nervous system permeability	–2.777 log PS
Metabolism	CYP2D6 substrate	No
	CYP3A4 substrate	Yes
	CYP1A2 inhibitor	No
	CYP2C19 inhibitor	No
	CYP2C9 inhibitor	Yes
	CYP2D6 inhibitor	No
	CYP3A4 inhibitor	No
Excretion	Total clearance	0.15 log ml/kg/day
	Renal OCT2 substrate	No
Toxicity	AMES toxicity	No
	hERG I and II inhibitor	No
	Hepatotoxicity	Yes
	Skin sensitisation	No

so far, namely because the cells themselves have low to no expression of certain important receptors like estrogen receptors, progesterone receptors and the human epidermal growth factor receptors. Consequently, hormonal therapy and drugs that target these receptors are ineffective. It has become increasingly important to develop new, alternative methods for treating this highly invasive and aggressive type of cancer. The results presented in this study could provide a framework for the development of novel targeted thiohydantoin based anticancer pharmaceuticals.

Data availability statement

All data related to this investigation is contained within the manuscript and supplementary material. Any further inquiries can be directed to the corresponding author.

Funding and acknowledgements

The authors are grateful to the Ministry of science, technological development and innovation of the Republic of Serbia for support (contract numbers 451-03-33/2026-03/200378, 451-03-137/2025-03/200111 and 451-03-136/2025-03/200026). No outside funding was received for research included in this paper.

Conflict of interest

The authors declare that they have no known competing financial interests or personal relationships that could have appeared to influence the work reported in this paper.

5. References

1. A. Upadhyay, *Genes Dis.* **2021**, *8*, 655–661. **DOI**:10.1016/j.gendis.2020.09.002
2. F. Bray, M. Laversanne, H. Sung, J. Ferlay, R. L. Siegel, I. Soerjomataram, A. Jemal, *CA. Cancer J. Clin.* **2024**, *74*, 229–263. **DOI**:10.3322/caac.21834
3. R. Hong, B. Xu, *Cancer Commun.* **2022**, *42*, 913–936. **DOI**:10.1002/cac2.12358
4. L. Konnert, F. Lamaty, J. Martinez, E. Colacino, *Chem. Rev.* **2017**, *117*, 13757–13809. **DOI**:10.1021/acs.chemrev.7b00067
5. M. A. Metwally, E. Abdel-Latif, *J. Sulfur Chem.* **2012**, *33*, 229–257. **DOI**:10.1080/17415993.2011.643550
6. S. H. Cho, S. H. Kim, D. Shin, *Eur. J. Med. Chem.* **2019**, *164*, 517–545. **DOI**:10.1016/j.ejmech.2018.12.066
7. S. M. Khirallah, H. M. M. Ramadan, A. Shawky, S. H. Qahl, R. S. Baty, N. Alqadri, A. M. Alsuhaibani, M. Jaremko, A.-H. Emwas, E. M. Saied, *Molecules* **2022**, *27*, 6271. **DOI**:10.3390/molecules27196271
8. M. Su, D. Xia, P. Teng, A. Nimmagadda, C. Zhang, T. Odom, A. Cao, Y. Hu, J. Cai, *J. Med. Chem.* **2017**, *60*, 8456–8465. **DOI**:10.1021/acs.jmedchem.7b00847
9. J. Tchekalarova, P. Todorov, T. Stoyanova, M. Atanasova, *Int. J. Mol. Sci.* **2023**, *24*, 16071. **DOI**:10.3390/ijms242216071
10. S. M. Khirallah, H. M. M. Ramadan, H. A. A. Aladl, N. O. Ayaz, L. A. F. Kurdi, M. Jaremko, S. Z. Alshawwa, E. M. Saied, *Pharmaceuticals* **2022**, *15*, 1576. **DOI**:10.3390/ph15121576
11. A. Czopek, M. Kubacka, A. Bucki, A. Siwek, B. Filipek, M. Pawłowski, M. Kołaczkowski, *Pharmacol. Reports* **2021**, *73*, 1361–1372. **DOI**:10.1007/s43440-021-00284-6
12. D. Kim, L. Wang, C. G. Caldwell, P. Chen, P. E. Finke, B. Oates, M. MacCoss, S. G. Mills, L. Malkowitz, S. L. Gould, J. A. DeMartino, M. S. Springer, D. Hazuda, M. Miller, J. Kessler, R. Danzeisen, G. Carver, A. Carella, K. Holmes, J. Lineberger, W. A. Schleif, E. A. Emini, *Bioorg. Med. Chem. Lett.* **2001**, *11*, 3103–3106. **DOI**:10.1016/S0960-894X(01)00655-2
13. K. Virijevic, P. Stanic, J. Muskinja, J. Katanic-Stankovic, N. Sreckovic, M. Zivanovic, B. Smit, *J. Serb. Chem. Soc.* **2022**, *87*, 1349–1358. **DOI**:10.2298/JSC220404047V
14. L. Sacconnay, L. Ryckewaert, G. M. Randazzo, C. Petit, C. D. S. Passos, J. Jachno, V. Michailovienė, A. Zubrienė, D. Matulis, P.-A. Carrupt, C. A. Simões-Pires, A. Nurisso, *Eur. J. Pharm. Sci.* **2016**, *85*, 59–67. **DOI**:10.1016/j.ejps.2016.01.010
15. L. Ma, Y. Zhou, D. Yang, M.-W. Wang, W. Lu, J. Jin, *Molecules* **2022**, *27*, 5867. **DOI**:10.3390/molecules27185867
16. Y. S. Bae, S. Choi, J. J. Park, J. H. Joo, M. Cui, H. Cho, W. J. Lee, S. H. Lee, *Bioorg. Med. Chem.* **2016**, *24*, 4144–4151. **DOI**:10.1016/j.bmc.2016.06.056
17. F. Wu, H. Jiang, B. Zheng, M. Kogiso, Y. Yao, C. Zhou, X.-N. Li, Y. Song, *J. Med. Chem.* **2015**, *58*, 6899–6908. **DOI**:10.1021/acs.jmedchem.5b00684
18. P. Majumdar, C. Bathula, S. M. Basu, S. K. Das, R. Agarwal, S. Hati, A. Singh, S. Sen, B. B. Das, *Eur. J. Med. Chem.* **2015**, *102*, 540–551. **DOI**:10.1016/j.ejmech.2015.08.032
19. E. Żesławska, A. Kincses, G. Spengler, W. Nitek, K. Wyrzuc, K. Kieć-Kononowicz, J. Handzlik, *Bioorg. Med. Chem.* **2016**, *24*, 2815–2822. **DOI**:10.1016/j.bmc.2016.04.055
20. K. Gallop, *Emerg. Med. Australas.* **2010**, *22*, 108–118. **DOI**:10.1111/j.1742-6723.2010.01269.x
21. W. Kassouf, S. Tanguay, A. G. Aprikian, *J. Urol.* **2003**, *169*, 1742–1744. **DOI**:10.1097/01.ju.0000057795.97626.66
22. Z. T. Al-Salama, *Drugs* **2018**, *78*, 699–705. **DOI**:10.1007/s40265-018-0900-z
23. I. D. Davis, A. J. Martin, M. R. Stockler, S. Begbie, K. N. Chi, S. Chowdhury, X. Coskinas, M. Frydenberg, W. E. Hague, L. G. Horvath, A. M. Joshua, N. J. Lawrence, G. Marx, J. McCaffrey, R. McDermott, M. McJannett, S. A. North, F. Parnis, W. Parulekar, D. W. Pook, M. N. Reaume, S. K. Sandhu, A. Tan, T. H. Tan, A. Thomson, E. Tu, F. Vera-Badillo, S. G. Williams, S. Yip, A. Y. Zhang, R. R. Zielinski, C. J. Sweeney, *N. Engl. J. Med.* **2019**, *381*, 121–131. **DOI**:10.1056/NEJMoa1903835
24. V. Ivasiv, C. Albertini, A. E. Gonçalves, M. Rossi, M. L. Bolognesi, *Curr. Top. Med. Chem.* **2019**, *19*, 1694–1711. **DOI**:10.2174/1568026619666190619115735
25. S. Majhi, D. Das, *Tetrahedron* **2021**, *78*, 131801. **DOI**:10.1016/j.tet.2020.131801
26. B. Ahmad, M. U. Rehman, I. Amin, A. Arif, S. Rasool, S. A. Bhat, I. Afzal, I. Hussain, S. Bilal, M. ur R. Mir, *Sci. World J.*

2015. **DOI**:10.1155/2015/816364
27. X. Cao, C. Chen, K. Yin, T. Wang, Y. Huang, P. Chen, P. Su, *J. Biochem. Mol. Toxicol.* **2024**, *38*, e70074. **DOI**:10.1002/jbt.70074
28. A. C. Garrido-Castro, N. U. Lin, K. Polyak, *Cancer Discov.* **2019**, *9*, 176–198. **DOI**:10.1158/2159-8290.CD-18-1177
29. L. R. Smith, *Chem. Educ.* **1996**, *1*, 1–18. **DOI**:10.1007/s00897960034a
30. J. S. Buck, *Org. Synth.* **1933**, *13*, 102. **DOI**:10.15227/orgsyn.013.0102
31. A. R. Katritzky, Q. Long, H. Y. He, G. Qiua, A. L. Wilcox, *Arkivoc* **2000**, *2000*, 868–875. **DOI**:10.3998/ark.5550190.0001.603
32. B. Šmit, R. Z. Pavlović, A. Radosavljević-Mihailović, A. Došen, D. S. Šeklić, M. N. Živanović, *J. Serb. Chem. Soc.* **2013**, *78*, 217–227. **DOI**:10.2298/JSC120725154S
33. K. Hostanska, G. Jürgenliemk, G. Abel, A. Nahrstedt, R. Saller, *Cancer Detect. Prev.* **2007**, *31*, 129–139. **DOI**:10.1016/j.cdp.2007.03.001
34. T. Mosmann, *J. Immunol. Methods* **1983**, *65*, 55–63. **DOI**:10.1016/0022-1759(83)90303-4
35. A. Tarushi, E. Polatoglou, J. Kljun, I. Turel, G. Psomas, D. P. Kessissoglou, *Dalton Trans.*, **2011**, *40*, 9461. **DOI**:10.1039/c1dt10870k
36. G. Zhang, Y. Ma, *Food Chem.* **2013**, *136*, 442–449. **DOI**:10.1016/j.foodchem.2012.09.026
37. M. J. Frisch, G. W. Trucks, H. B. Schlegel, G. E. Scuseria, M. A. Robb, J. R. Cheeseman, G. Scalmani, V. Barone, B. Mennucci, G. A. Petersson, H. Nakatsuji, M. Caricato, X. Li, H. P. Hratchian, A. F. Izmaylov, J. Bloino, G. Zheng, J. L. Sonnenberg, M. Hada, M. Ehara, K. Toyota, R. Fukuda, J. Hasegawa, M. Ishida, T. Nakajima, Y. Honda, O. Kitao, H. Nakai, T. Vreven, J. A. Montgomery, J. E. Peralta, F. Ogliaro, M. Bearpark, J. J. Heyd, E. Brothers, K. N. Kudin, V. N. Staroverov, R. Kobayashi, J. Normand, K. Raghavachari, A. Rendell, J. C. Burant, S. S. Iyengar, J. Tomasi, M. Cossi, N. Rega, N. J. Millam, M. Klene, J. E. Knox, J. B. Cross, V. Bakken, C. Adamo, J. Jaramillo, R. Gomperts, R. E. Stratmann, O. Yazyev, A. J. Austin, R. Cammi, C. Pomelli, J. W. Ochterski, R. L. Martin, K. Morokuma, V. G. Zakrzewski, G. A. Voth, P. Salvador, J. J. Dannenberg, S. Dapprich, A. D. Daniels, Ö. Farkas, J. B. Foresman, J. V. Ortiz, J. Cioslowski, D. J. Fox, *Gaussian 09, Revision C.01*, Gaussian, Inc., Wallingford CT, **2009**.
38. O. Trott, A. J. Olson, *J. Comput. Chem.* **2010**, *31*, 455–461. **DOI**:10.1002/jcc.21334
39. S. K. Burley, H. M. Berman, C. Bhikadiya, C. Bi, L. Chen, L. Di Costanzo, C. Christie, J. M. Duarte, S. Dutta, Z. Feng, S. Ghosh, D. S. Goodsell, R. K. Green, V. Guranovic, D. Guzenko, B. P. Hudson, Y. Liang, R. Lowe, E. Peisach, I. Periskova, C. Randle, A. Rose, M. Sekharan, C. Shao, Y.-P. Tao, Y. Valasatava, M. Voigt, J. Westbrook, J. Young, C. Zardecki, M. Zhuravleva, G. Kurisu, H. Nakamura, Y. Kengaku, H. Cho, J. Sato, J. Y. Kim, Y. Ikegawa, A. Nakagawa, R. Yamashita, T. Kudou, G.-J. Bekker, H. Suzuki, T. Iwata, M. Yokochi, N. Kobayashi, T. Fujiwara, S. Velankar, G. J. Kleywegt, S. Anyango, D. R. Armstrong, J. M. Berrisford, M. J. Conroy, J. M. Dana, M. Deshpande, P. Gane, R. Gáborová, D. Gupta, A. Gutmanas, J. Koča, L. Mak, S. Mir, A. Mukhopadhyay, N. Nadzirin, S. Nair, A. Patwardhan, T. Paysan-Lafosse, L. Pravda, O. Salih, D. Sehnal, M. Varadi, R. Vařeková, J. L. Markley, J. C. Hoch, P. R. Romero, K. Baskaran, D. Maziuk, E. L. Ulrich, J. R. Wedell, H. Yao, M. Livny, Y. E. Ioannidis, *Nucleic Acids Res.* **2019**, *47*, D520–D528. **DOI**:10.1093/nar/gky949
40. Dassault Systemes BIOVIA. Discovery Studio Modelling Environment (Release 2017); Dassault Systemes. San Diego, CA, USA, **2016**.
41. A. Daina, O. Michielin, V. Zoete, *Sci. Rep.* **2017**, *7*, 42717. **DOI**:10.1038/srep42717
42. D. E. V. Pires, T. L. Blundell, D. B. Ascher, *J. Med. Chem.* **2015**, *58*, 4066–4072. **DOI**:10.1021/acs.jmedchem.5b00104
43. F. Yang, Y. Zhang, H. Liang, *Int. J. Mol. Sci.* **2014**, *15*, 3580–3595. **DOI**:10.3390/ijms15033580
44. P. A. Galkina, M. A. Proskurnin, *Appl. Organomet. Chem.* **2018**, *32*, e4150. **DOI**:10.1002/aoc.4150
45. X. Wang, X. Xie, C. Ren, Y. Yang, X. Xu, X. Chen, *Food Chem.* **2011**, *127*, 705–710. **DOI**:10.1016/j.foodchem.2010.12.128
46. J. R. Lakowicz, in: J. R. Lakowitz (Ed.): Principles of Fluorescence Spectroscopy, Springer US, Boston, MA, USA, **2006**. **DOI**:10.1007/978-0-387-46312-4
47. J. R. Lakowicz, G. Freshwater, G. Weber, *Biophys. J.* **1980**, *32*, 591–601. **DOI**:10.1016/S0006-3495(80)84992-7
48. S.-S. Wu, W.-B. Yuan, H.-Y. Wang, Q. Zhang, M. Liu, K.-B. Yu, *J. Inorg. Biochem.* **2008**, *102*, 2026–2034. **DOI**:10.1016/j.jinorgbio.2008.08.005
49. R. Esteghamat-Panah, H. Hadadzadeh, H. Farrokhpour, J. Simpson, A. Abdolmaleki, F. Abyar, *Eur. J. Med. Chem.* **2017**, *127*, 958–971. **DOI**:10.1016/j.ejmech.2016.11.005
50. F. Zsila, *Mol. Pharm.* **2013**, *10*, 1668–1682. **DOI**:10.1021/mp400027q
51. Z. Wang, J. X. Ho, J. R. Ruble, J. Rose, F. Rüker, M. Ellenburg, R. Murphy, J. Click, E. Soistman, L. Wilkerson, D. C. Carter, *Biochim. Biophys. Acta Gen. Subj.* **2013**, *1830*, 5356–5374. **DOI**:10.1016/j.bbagen.2013.06.032
52. A. Rilak Simović, R. Masnikosa, I. Bratsos, E. Alessio, *Coord. Chem. Rev.* **2019**, *398*, 113011. **DOI**:10.1016/j.ccr.2019.07.008
53. M. Sirajuddin, S. Ali, A. Badshah, *J. Photochem. Photobiol. B Biol.* **2013**, *124*, 1–19. **DOI**:10.1016/j.jphotobiol.2013.03.013
54. A. Wolfe, G. H. Shimer, T. Meehan, *Biochemistry* **1987**, *26*, 6392–6396. **DOI**:10.1021/bi00394a013
55. V. Brabec, J. Kasparkova, *Coord. Chem. Rev.* **2018**, *376*, 75–94. **DOI**:10.1016/j.ccr.2018.07.012
56. M. Međedović, A. Rilak Simović, D. Ćoćić, L. Senft, S. Matić, D. Todorović, S. Popović, D. Baskić, B. Petrović, *Dalton Trans.* **2023**, *52*, 1323–1344. **DOI**:10.1039/D2DT02993F
57. R.-W. C. Yen, P. M. Vertino, B. D. Nelkin, J. J. Yu, W. El-Deiry, A. Cumaraswamy, G. G. Lennon, B. J. Trask, P. Celano, S. B. Baylin, *Nucleic Acids Res.* **1992**, *20*, 2287–2291. **DOI**:10.1093/nar/20.9.2287
58. L. Yan, Q. Geng, Z. Cao, B. Liu, L. Li, P. Lu, L. Lin, L. Wei, Y. Tan, X. He, L. Li, N. Zhao, C. Lu, *Biomed. Pharmacother.* **2023**, *168*, 115753. **DOI**:10.1016/j.biopha.2023.115753

59. J. Song, M. Teplova, S. Ishibe-Murakami, D. J. Patel, *Science* **2012**, *335*, 709–712. **DOI**:10.1126/science.1214453

Povzetek

Povzetek: Ta študija preučuje serijo zingeron 2-tiohidantoinov z vidika protirakavega delovanja proti človeškemu adenokarcinomu dojke ter raziskuje možne mehanizme protirakavega delovanja. Citotoksičnost je bila testirana na visoko invazivnih trojno negativnih rakavih celicah dojke MDA-MB-231 in na zdravih celicah MRC-5. Najbolj učinkovina spojina **2e** je pokazala izrazit citotoksični učinek na rakave celice dojke, medtem ko na zdravih celicah ni izkazala merljive toksičnosti. Fluorescenčne meritve interakcij s človeškim serumskim albuminom, skupaj z molekularnim sidranjem, so pokazale močno vezavo in dobre transportne sposobnosti, kar nakazuje dobro biološko razpoložljivost. Fluorescenčne in hidrodinamične meritve z DNK so pokazale nižjo afiniteto vezave, kar nakazuje, da so za protirakavo delovanje odgovorne proteinske tarče. Izvedeno je bilo temeljito molekularno sidranjev v 36 možnih proteinskih tarč adenokarcinoma dojke, rezultati pa nakazujejo kompetitivno inhibicijo DNA-metiltransferaze 1 kot mehanizem protirakavega delovanja. Analiza ADMET je napovedala ugodne fizikalno-kemijske in farmakokinetične lastnosti.